MRS Advances © 2018 Materials Research Society
DOI: 10.1557/adv.2018.404

Fabrication and Surface Engineering of Two-Dimensional SnS Toward Piezoelectric Nanogenerator Application

Naoki Higashitarumizu[1], Hayami Kawamoto[1], Keiji Ueno[2] and Kosuke Nagashio[1,3]

[1]*Department of Materials Engineering, The University of Tokyo, 7-3-1 Hongo, Bunkyo, Tokyo 113-8656, Japan*

[2]*Department of Chemistry, Graduate School of Science and Engineering, Saitama University, 255 Shimo-Okubo, Sakura, Saitama 338-8570, Japan*

[3]*PRESTO, Japan Science and Technology Agency (JST), Tokyo 113-8656, Japan*

ABSTRACT

Mechanical exfoliation is performed to fabricate ultrathin SnS layers, and chemical/thermal stability of SnS layers is discussed in comparison with GeS, toward piezoelectric nanogenerator application. Both SnS and GeS are difficult to be exfoliated under 10 nm using tape exfoliation due to strong interlayer ionic bonding by lone pair electrons in Sn or Ge atoms. Au-mediated exfoliation enables to fabricate larger-scale ultrathin SnS and GeS layers thinner than 10 nm owing to strong semi-covalent bonding between Au and S atoms, but GeS surface immediately degrades during Au etching in an oxidative KI/I_2 solution. Although the surface of SnS after the Au-mediated exfoliation reveals several-nm oxide layer of SnO_x, the surface morphology retains the flatness unlike the case of GeS. The SnS layers are more robust than GeS against the thermal annealing as well as the chemical treatment, suggesting that SnO_x works as a passivation layer for SnS. Self-passivated SnS monolayer can be obtained by a controlled post-oxidation.

INTRODUCTION

Two-dimensional tin sulfide (SnS), one of the group-IV monochalcogenides (MXs; M=Sn/Ge and X=S/Se), has recently attracted interests in the application to flexible piezoelectric generator, because it is theoretically predicted that SnS has a large piezoelectric coefficient d_{11}=145 pm/V that is comparable to conventional lead zirconate titanate (PZT, d_{33}~300 pm/V) [1]. For MXs, the piezoelectricity exists only in the odd-number layers, since the broken inversion symmetry disappears in the even-number layers. The piezoelectric coefficient increases with decreasing the layer number, and is

maximized in the monolayer [2]. However, the fabrication of monolayer SnS has only been achieved by liquid phase exfoliation with smaller lateral size than 500 nm [3]. Although relatively large SnS layers can be fabricated by mechanical exfoliation and thin film growth methods, SnS layers thinner than 5.5 nm have not been realized yet [4]. This is probably due to the strong interlayer interaction by lone pair electrons in Sn atoms [5].

Figure 1(a) shows the relationship between the activation energy barrier for O_2 molecule to chemisorb on the monolayer MXs or black phosphorus (BP) [6], and the elastic energy barrier of these materials which is related to the order-disorder transition [7]. The order-disorder transition indicates the structural stability. There is a trade-off between the structural stability and the resistance against oxidation. In MXs, GeS is the only material which is structurally stable at room temperature (RT), but is the most oxidizable material. In contrast, SnS is the most structurally unstable material in MXs, while has the largest resistance against oxidation. Figure 1(b) shows melting temperatures of two-dimensional materials (SnS, GeS, BP and MoS_2) and their oxides (SnO_2, GeO, P_2O_5 and MoO_3). For the Ge oxides, GeO is known to easily desorb at low temperature of 400–600˚C [8,9]. SnS, GeS and BP are more unstable than MoS_2, though SnO_2 is more stable than any other oxide materials. Thermally unstable materials tend to be easily decomposed with chemical reaction even at RT owing to the weak bonding energy between constituent elements. On the other hand, it can be expected that SnO_2 works as a stable passivation layer for SnS layers. The thermal and the chemical stabilities of SnS and SnO_x, however, have not been investigated experimentally. Fundamental understanding is required on the stability of ultrathin SnS layers toward the realization of its piezoelectric device.

In this study, Au-mediated mechanical exfoliation is used to fabricate ultrathin SnS layers. For MoS_2, Au-mediated exfoliation has been found to be effective to fabricate a large-scale monolayer owing to the strong semi-covalent bonds between Au and S atoms [10]. In the Au-mediated exfoliation process, a KI/I_2 oxidative solution is used to etch the Au residue, which might oxidize the SnS surface. In order to evaluate the chemical/thermal stabilities of SnS layers, effects of the chemical oxidation and laser annealing are studied on SnS layers in comparison with GeS.

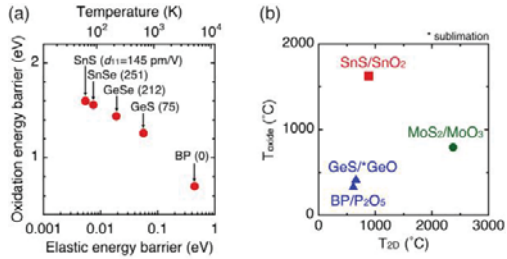

Figure 1. (a) The relationship between activation barrier energy for O_2 molecule to chemisorb on the material surface [6] and elastic energy barrier (E_e) which is related to the order-disorder transition [7] for monolayers of group-IV monochalcogenides and black phosphorus. The top transverse axis is obtained by dividing E_e by the Boltzmann constant. Calculated piezoelectric coefficients d_{11} (pm/V) [1] are also shown. (b) Melting temperatures of two-dimensional materials (T_{2D}) and oxide materials (T_{oxide}).

EXPERIMENTAL DETAILS

SnS and GeS thin layers were transferred on 90-nm SiO_2/n^+-Si substrates by the tape exfoliation and the Au-mediated exfoliation. In the Au-mediated exfoliation, the Au residue was etched in the KI/I_2 solution for 5 min, followed by a rinse in deionized water. The thickness and surface morphology were measured by atomic force microscopy (AFM). In order to investigate the effect of the Au etchant on the surface oxidation of exfoliated thin layers, Auger electron spectroscopy (AES) and X-ray photoelectron spectroscopy (XPS) were used.

Micro-Raman spectra of the tape-exfoliated bulk SnS and GeS were measured in air at RT. The excitation laser wavelength and power were 488 nm and 5.3 μW, respectively. Magnification of the objective lens to irradiate sample surface was ×100, and the laser diameter on the surface ($1/e^2$ intensity in the Gaussian-shaped spatial distribution) was normally 1 μm. The laser annealing (LA) was performed in air for the tape-exfoliated bulk SnS and GeS to evaluate the thermal stability. The laser was irradiated in air for 1 min with the same system of the Raman measurement. The power of LA was changed between 5.3 and 5.9×10^3 μW. After the LA, a Raman spectrum at the annealed spot was measured with the laser power of 5.3 μW.

RESULTS AND DISCUSSION

Tape exfoliation versus Au-mediated exfoliation

Figure 2(a) shows an optical image of tape-exfoliated SnS flakes. The typical size and thickness were several μm and several tens of nm, respectively, as shown in Figure 2(e). By the Au-mediated exfoliation, much larger SnS flakes were obtained, compared to the tape exfoliation, as shown in Figure 2(b). The flake thickness exhibits a wide distribution down to 1.1 nm, which is close to the thickness of monolayer SnS (~0.6 nm), as shown in Figure 2(e). This relatively larger ultrathin SnS flake can be attributed to the strong semi-covalent bonding between Au and S atoms. AFM images of thin flakes by the tape exfoliation and the Au-mediated exfoliation are shown in Figures 2(c) and 2(d), respectively. Atomically flat surfaces were obtained for thin flakes with both exfoliation methods. Typical RMS roughness of the bulk flakes by tape exfoliation and Au-mediated exfoliation were 0.07 and 0.13 nm, respectively.

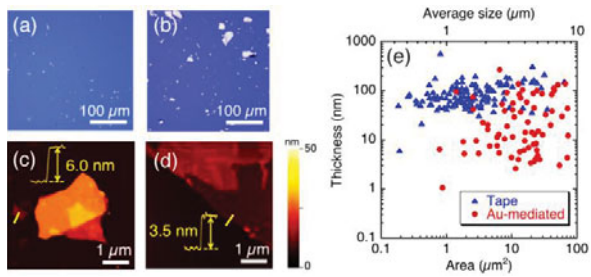

Figure 2. Optical images of SnS flakes obtained by (a) tape exfoliation and (b) Au-mediated exfoliation, and AFM topographic images of SnS flakes obtained by (c) tape exfoliation and (d) Au-mediated exfoliation. (e) The relationship between thickness and surface area of exfoliated SnS flakes. Average size is calculated as the square root of the surface area.

Chemical stabilities of SnS and GeS

Au-mediated exfoliation was not applicable to GeS unlike SnS due to the surface degradation as described below. In order to investigate the effects of the Au etchant on the surface of SnS and GeS, tape-exfoliated layers were dipped in the Au etchant for 5 min. Figures 3(a)–3(d) compare the morphology of bulk SnS and GeS flakes before and after the Au etchant treatment. Even after the Au etchant treatment, the SnS flake maintained a flat surface as shown in Figure 3(c), while the GeS surface was etched ununiformly as shown in Figure 3(d). Typical Raman spectra of the tape-exfoliated bulk SnS and GeS are shown at the bottom of Figures 3(f) and 3(g), respectively. For SnS, two Raman peaks are observed at 162.0 and 191.2 cm^{-1}. These values agree with the reported values [11]. Although other specific peaks of SnS at around 96 and 220 cm^{-1} [11] were not observed due to the detection limit at the excitation power of 5.3 μW, those peaks were certainly observed under the strong excitation at 500 μW. On the other hand, for GeS, four Raman peaks were observed at 111.7, 213.7, 237.3, and 269.9 cm^{-1}. These values agree with the reported values [12]. After the Au etchant treatment, there was no change in the spectrum shape of SnS, whereas for GeS, an additional broad peak was clearly observed at ~370 cm^{-1}, as shown in Figures 3(f) and 3(g). The additional peak is very similar with the Raman spectrum of GeO_xS_y [13], indicating the existence of an oxide layer. The chemical etching of GeS in Figure 3(d) is probably attributed to the low oxidation energy barrier and the chemical instability of GeO_x as shown in Figure 1(b). Additionally, GeO_2 dissolves in the water even at RT. When the Au-mediated exfoliation was used for GeS, worm-eaten thin layers were obtained as shown in Figure 3(e).

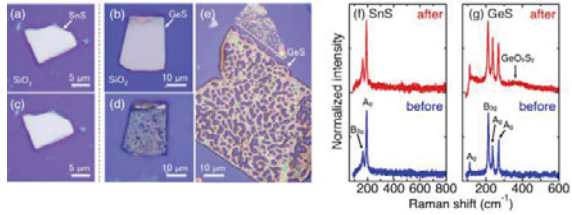

Figure 3. (a, b) Optical images of tape-exfoliated bulk flakes of SnS and GeS. (c, d) Optical images of SnS and GeS treated in the Au etchant for 5 min. (e) Optical image of GeS after Au-mediated exfoliation. (f, g) Typical Raman spectra of tape-exfoliated bulk SnS and GeS before/after the Au etchant treatment for 5 min.

Compared with GeS, it is evident that SnS is chemically stable. To further investigate the origin of the chemical stability of SnS in detail, AES measurements were carried out for bulk and 3.5nm-thick flakes obtained by the Au-mediated exfoliation. As shown in Figure 4(a), the Auger signals of Sn and S were detected for the bulk SnS, while for the 3.5nm-thick flake, only the Sn signal was observed and the S signal was missing. In this measurement, the probe acquisition depth is deeper than flake thickness since the signal from SiO_2 substrate was detected. AES results suggest that the flakes thinner than 3.5 nm obtained by the Au-mediated exfoliation are totally oxidized. Figure 4(b) shows typical XPS spectra of bulk SnS obtained by the tape exfoliation and the Au-mediated exfoliation. For the tape-exfoliated SnS, a clear Sn $3d_{5/2}$ peak was observed with slight asymmetry. The asymmetric shape is caused by the surface oxidation due to air exposure or/and residual oxygen in the XPS chamber. By Gaussian fitting with binding energies of Sn-S (486.6 eV) and Sn-O (487.4) from the reference values [14], the intensity ratio I_{SnO}/I_{SnS} for the raw data was determined to be 0.1. For the Au-mediated exfoliation, a strong additional peak was observed at 487.4 eV, which corresponds to the binding energy of Sn-O. The ratio I_{SnO}/I_{SnS} for the raw data was determined to be 3.2,

which is much larger than that of the tape-exfoliated SnS. Although the SnS surface was oxidized after the Au-mediated exfoliation, the Sn $3d_{5/2}$ peak from Sn-S was still observed as well as the peaks of S $2p_{3/2}$ (~162 eV) and S $2p_{1/2}$ (~163 eV), indicating that the oxidized layer was limited within the escape depth of photoelectrons; several nm in thickness. These results suggest that the surface oxidation of SnS is self-limited unlike the case of GeS.

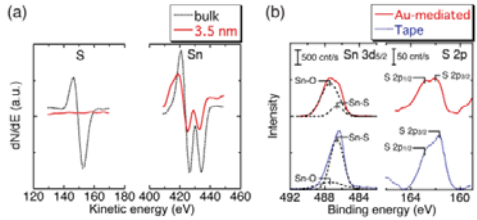

Figure 4. (a) Typical differential AES spectra for bulk and 3.5nm-thick SnS after the Au-mediated exfoliation. (b) Typical XPS spectra of Sn 3d and S 2p for bulk SnS after the tape and Au-mediated exfoliation. Dashed lines represent Gaussian fits to the data, with the binding energies of SnS and SnO [14].

Thermal stabilities of SnS and GeS

Figure 5(a) shows typical Raman spectra of SnS after the LA at different laser powers between 5.3 and 5.9×10^3 μW. With increasing the LA power, the peak intensity and the full-width at half maximum (FWHM) were constant up to 1.2×10^3 μW. However, the peak intensity decreased over 1.7×10^3 μW as shown in Figure 5(c), with increased FWHM. After the LA at 5.9×10^3 μW, the peak intensity decreased to ~20% of 5.3 μW and the Raman peak from the Si substrate was observed at ~518 cm^{-1}. These results indicate that the upper layers of bulk SnS evaporated due to the excess heating with the stronger LA power than 1.7×10^3 μW.

On the other hand, the Raman spectrum of GeS was found to be easily degraded after the LA; the Raman intensity decreased over 57.7 μW, which is much lower than the critical LA power for SnS; 1.7×10^3 μW. After the LA at 5.9×10^3 μW, Raman peaks from GeS disappeared as shown in Figure 5(b). In addition to the narrow Si peak at ~518 cm^{-1}, a sharp peak at ~299 cm^{-1} appeared, which is possibly from the Ge-Ge bond. Moreover, a peak of GeO_xS_y was observed at ~376 cm^{-1} in the same way as the GeS oxidized in the Au etchant (Figure 3(g)).

Based on these results, SnS is revealed to be chemically and thermally stable. The key feature is the formation of the SnO_x passivation layer on the SnS flake, which is chemically and thermally stable because of its high melting temperature of 1630˚C (SnO_2) or 1080˚C (SnO) [15]. This is completely opposite situation from GeS, where

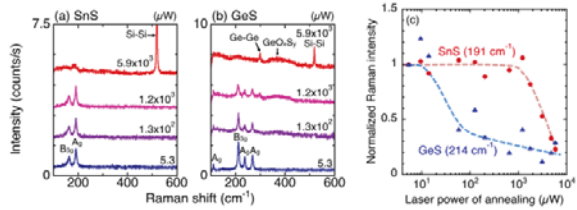

Figure 5. (a, b) Typical Raman spectra of laser-annealed bulk SnS and GeS flakes. The laser annealing was performed in air under different laser powers between 5.3 and 5.9×10^3 μW. The laser power for Raman measurement was fixed at 5.3 μW. (c) Normalized Raman intensity versus laser power of annealing for bulk SnS and GeS. The dashed lines are guides to the eye.

GeO is quite unstable. So far, in the case of BP and WSe_2, layer-by-layer oxidations have been realized by oxygen plasma [16] and ozone treatment [17], respectively, since the oxidation rate is limited by the oxygen diffusion in the oxide layer when the oxide thickness is moderately increased. Therefore, monolayer SnS self-passivated with the SnO_x layer will be realized by precisely controlling the surface oxidation.

CONCLUSIONS

Au-mediated exfoliation of SnS and GeS, and chemical/thermal stability of exfoliated flakes were investigated. The Au-mediated exfoliation enabled relatively large SnS layers thinner than 10 nm, but is not applicable for GeS due to unstable surface oxides during the Au etching process. Although the SnS surface is also oxidized, SnO_x is much stable and the oxidation is self-limited. As well as the chemical stability, SnS also shows thermal stability owing to the robust SnO_x layer that works as the passivation layer. The present findings indicate that SnO_x/SnS hetero-structure is a promising candidate for the nanogenerator.

ACKNOWLEDGMENTS

This research was supported by the JSPS Core-to-Core Program, A. Advanced Research Networks, JSPS KAKENHI Grant Numbers JP25107004, JP16H04343, JP16K14446, and JP26886003, and JST PRESTO Grant Number JPMJPR1425, Japan.

REFERENCES

1. R. Fei, W. Li, J. Li and L. Yang, *Appl. Phys. Lett.* **107**, 173104 (2015).
2. W. Wu, L. Wang, Y. Li, F. Zhang, L. Lin, S. Niu, D. Chenet, X. Zhang, Y. Hao, T. F. Heinz, J. Hone and Z. L. Wang, *Nature* 514, 470 (2014).
3. Y. Sun, Z. Sun, S. Gao, H. Cheng, Q. Liu, F. Lei, S. Wei, and Y. Xie, *Adv. Energy Mater.* **4**, 1300611 (2014).
4. J. Xia, X. -Z. Li, X. Huang, N. Mao, D. -D. Zhu, L. Wang, H. Xu and X. -M. Meng, *Nanoscale* **8**, 2063 (2016).
5. H. -Y. Song and J. -T. Lü, *Chem. Phys. Lett.* **695**, 200 (2018).
6. Y. Guo, S. Zhou, Y. Bai and J. Zhao, *ACS Appl. Mater. Interfaces* **9**, 12013 (2017).
7. M. Mehboudi, A. M. Dorio, W. Zhu, A. Van Der Zande, H. O. H. Churchill, A. A. Pacheco-Sanjuan, E. O. Harriss, P. Kumar and S. Barraza-Lopez, *Nano Lett.* **16**, 1704 (2016).
8. K. Prabhakaran, F. Maeda, Y. Watanabe and T. Ogino, *Thin Solid Films* **369**, 289 (2000).
9. K. Kita, C. H. Lee, T. Tabata, T. Nishimura, K. Nagashio and A. Toriumi, *J. Appl. Phys.* **108**, 54104 (2010).
10. S. B. Desai, S. R. Madhvapathy, M. Amani, D. Kiriya, M. Hettick, M. Tosun, Y. Zhou, M. Dubey, J. W. Ager, D. Chrzan and A. Javey, *Adv. Mater.* **28**, 4053 (2016).
11. H. R. Chandrasekhar, R. G. Humphreys, U. Zwick and M. Cardona, *Phys. Rev. B* **15**, 2177 (1977).
12. J. D. Wiley, W. J. Buckel and R. L. Schmidt, *Phys. Rev. B* **13**, 2489 (1976).
13. C. Maurel, T. Cardinal, P. Vinatier, L. Petit, K. Richardson, N. Carlie, F. Guillen, M. Lahaye, M. Couzi, F. Adamietz, V. Rodriguez, F. Lagugné-Labarthet, V. Nazabal, A. Royon, and L. Canioni, *Mater. Res. Bull.* **43**, 1179 (2008).
14. W. E. Morgan and J. R. Van Wazer, *J. Phys. Chem.* **77**, 964 (1973).
15. D. R. Lide, *CRC handbook of chemistry and physics*, 79th ed. (CRC Press, New York, 1998) p. 4-90.
16. J. Pei, X. Gai, J. Yang, X. Wang, Z. Yu, D.-Y. Choi, B. Luther-Davies, and Y. Lu, *Nat. Commun.* **7**, 10450 (2016).
17. M. Yamamoto, S. Dutta, S. Aikawa, S. Nakaharai, K. Wakabayashi, M.S. Fuhrer, K. Ueno, and K. Tsukagoshi, *Nano Lett.* **15**, 2067 (2015).